

Unraveling the impact of reverse currents on electrode stability in anion exchange membrane water electrolysis

Citation for published version (APA):

Guruprasad, N., van der Schaaf, J., & de Groot, M. T. (2024). Unraveling the impact of reverse currents on electrode stability in anion exchange membrane water electrolysis. *Journal of Power Sources*, 613, Article 234877. Advance online publication. <https://doi.org/10.1016/j.jpowsour.2024.234877>

Document license:
CC BY

DOI:
[10.1016/j.jpowsour.2024.234877](https://doi.org/10.1016/j.jpowsour.2024.234877)

Document status and date:
E-pub ahead of print: 01/09/2024

Document Version:
Publisher's PDF, also known as Version of Record (includes final page, issue and volume numbers)

Please check the document version of this publication:

- A submitted manuscript is the version of the article upon submission and before peer-review. There can be important differences between the submitted version and the official published version of record. People interested in the research are advised to contact the author for the final version of the publication, or visit the DOI to the publisher's website.
- The final author version and the galley proof are versions of the publication after peer review.
- The final published version features the final layout of the paper including the volume, issue and page numbers.

[Link to publication](#)

General rights

Copyright and moral rights for the publications made accessible in the public portal are retained by the authors and/or other copyright owners and it is a condition of accessing publications that users recognise and abide by the legal requirements associated with these rights.

- Users may download and print one copy of any publication from the public portal for the purpose of private study or research.
- You may not further distribute the material or use it for any profit-making activity or commercial gain
- You may freely distribute the URL identifying the publication in the public portal.

If the publication is distributed under the terms of Article 25fa of the Dutch Copyright Act, indicated by the "Taverne" license above, please follow below link for the End User Agreement:

www.tue.nl/taverne

Take down policy

If you believe that this document breaches copyright please contact us at:

openaccess@tue.nl

providing details and we will investigate your claim.



Unraveling the impact of reverse currents on electrode stability in anion exchange membrane water electrolysis



Naveen Guruprasad^{a,b}, John van der Schaaf^{a,b}, Matheus T. de Groot^{a,b,*}

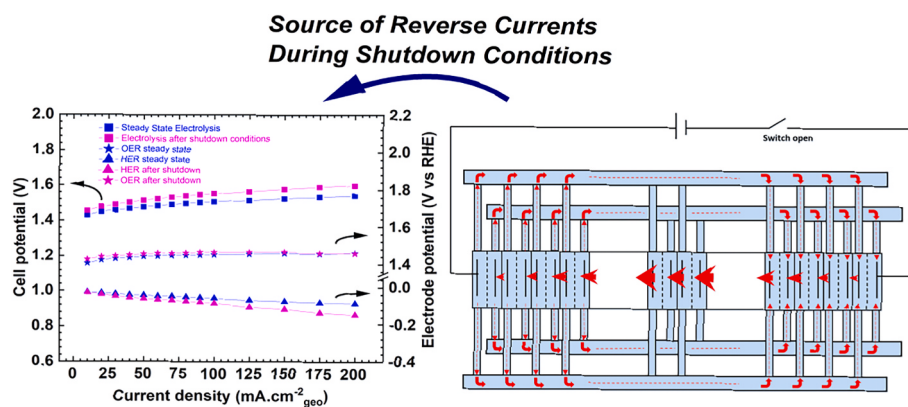
^a Department of Chemical Engineering and Chemistry, Sustainable Process Engineering Group, Eindhoven University of Technology, P.O. Box 513, Eindhoven, 5600, MB, the Netherlands

^b Eindhoven Institute for Renewable Energy Systems, Eindhoven University of Technology, PO Box 513, Eindhoven, 5600, MB, the Netherlands

HIGHLIGHTS

GRAPHICAL ABSTRACT

- Reverse currents during shutdown conditions can enhance electrode degradation.
- A reference electrode is employed to decouple individual electrode kinetics.
- Cathode catalysts showed higher susceptibility to degradation.



ARTICLE INFO

Keywords:

Anion exchange membrane electrolysis
Reverse currents
Electrode stability
Intermittent operation
Reference electrodes

ABSTRACT

Anion Exchange Membrane Water Electrolysis (AEMWE) stands out as one of the promising ways of producing green hydrogen. However, significant strides in performance and durability are necessary for commercial competitiveness. Shunt currents and reverse currents are common problems associated with electrolyzers using conductive liquid electrolytes during start/stop conditions and can enhance electrode degradation. This study incorporates a dual Pt-wire reference electrode within the flow cell consisting of a NiFe-layered double hydroxide anode and different cathode materials to decouple individual electrode kinetics under steady state and intermittent operating conditions. The performance of bimetallic cathode catalysts like PtRu/C and NiMo/C was assessed in comparison with traditional Pt/C catalysts in the context of the hydrogen evolution reaction. The initial observed catalyst activity displayed an evident trend in the order of PtRu/C > Pt/C > NiMo/C. When subjected to reverse currents, all three systems showed degradation in performance. The use of reference electrodes illustrated that all cathode coatings degraded as a result of the reverse currents while the anode remained relatively stable. The degradation followed the trend of NiMo/C > PtRu/C > Pt/C. This work thus shows that

* Corresponding author. Department of Chemical Engineering and Chemistry, Sustainable Process Engineering Group, Eindhoven University of Technology, P.O. Box 513, Eindhoven, 5600, MB, the Netherlands.

E-mail address: M.T.d.Groot@tue.nl (M.T. de Groot).

reverse currents are a real issue for AEMWE and demonstrates the importance of investigating electrodes under intermittent conditions.

1. Introduction

To address climate change and mitigate global emissions, expediting the shift from fossil fuels to renewable energies is crucial. However, the intermittent nature of renewables compels the development of safe and secure energy storage options to ensure a reliable and uninterrupted energy supply while minimizing curtailment. Power to gas is a promising concept that converts excess electrical power into grid-compatible gas. Hydrogen produced from water electrolysis has enormous potential for use as a green fuel or a chemical feedstock for many industrial processes [1,2]. The two well-established industrially relevant technologies are alkaline water electrolyzers (AWE) and proton exchange membrane water electrolyzers (PEMWE). Each of these technologies comes with its own set of limitations. AWEs traditionally operate at low current densities. They are relatively inflexible, i.e. they have a relatively high minimum load (10–40 % of nominal load) due to a high gas crossover through the porous separator [3–5]. On the other hand, the acidic environment of PEMWE presents a challenge as it necessitates the use of expensive materials for bipolar plates and porous transport layers (PTL) and noble metals like iridium and platinum as electrocatalysts.

Anion exchange membrane water electrolyzers (AEMWE) combine most of the advantages of AWE and PEMWE. AEMWE enables the choosing of inexpensive transition metal elements as electrocatalysts due to the alkaline environment [6]. It also allows dynamic operation at differential pressure conditions similar to PEMWE [7,8]. However, the technology still needs to be employed at a large scale as the performance and stability of the membrane electrode assembly (MEA) components, especially the catalysts, ionomers and the membrane, still need considerable improvement. One of the shortcomings of anion-exchange membranes (AEMs) is their low ionic conductivity compared to PEM membranes and susceptibility to degradation via nucleophilic substitution or Hofmann elimination at alkaline conditions and high temperatures [2,9,10]. This underscores the necessity for AEM and catalyst material enhancements to make it commercially competitive.

The oxygen evolution reaction (OER) in water electrolysis is a complex multistep reaction with sluggish kinetics, resulting in a substantial overpotential. Therefore, there is a need for better OER catalysts. In recent years, transition metal catalysts such as sulfides, phosphides, oxides and hydroxides have garnered significant attention due to their abundant availability and good performance. In particular, NiFe-layered double hydroxides (LDH) are known to have one of the lowest OER overpotentials in alkaline medium [11–13]. Although iridium oxide is considered the benchmark catalyst for OER in PEM electrolysis, many studies indicate that the activity of NiFe-LDH is superior to commercially available iridium and ruthenium oxide catalysts in an alkaline environment [14–16]. Furthermore, it is imperative to transition away from iridium due to its scarcity [17].

Conversely, compared to PEM systems, HER activity is almost two orders of magnitude slower in alkaline medium owing to higher hydrogen binding energies on the metal surface [18,19]. Due to its superior intrinsic activity, platinum is considered the benchmark HER catalyst in acidic and alkaline media. However, PtRu bimetallic catalysts have shown better activity for both HER and HOR in alkaline conditions [20,21]. Bimetallic catalysts like PtRu also address another challenge in AEM systems, i.e. minimizing undesired phenyl adsorption on the catalyst surface [22]. Phenyl groups are commonly present in the polymeric backbone of most ionomers due to their beneficial role in enhancing chemical stability under high pH conditions; however, recent studies indicate that phenyl oxidation of ionomers during electrolysis can cause a severe drop in performance [21,23,24].

Moreover, a high pH enables the use of Ni-based catalysts as an

alternative to Pt-based catalysts. Several studies suggest that NiMo is a promising candidate as it shows superior HER performance among non-PGM (platinum group metals) catalysts [2,16,25,26]. In this context, nickel serves as a good water dissociation centre, while molybdenum facilitates hydrogen adsorption.

Most studies on component characterization typically focus on standard electrolytic operation; however, system stability under intermittent operation is often overlooked. Bipolar alkaline/AEM systems can suffer stability problems due to repetitive startup/shutdown operating conditions. Fig. 1 shows a typical multi-cell electrolyzer stack configuration. Shunt currents or parasitic currents can manifest when the electrolyte is fed to the stack comprising numerous electrodes connected in series, thereby instigating potential gradients within the electrolyte and consequent ion migration, as shown by smaller red arrows within the manifold section in Fig. 1 (a). This process could lead to unintended corrosion of current collectors if poorly managed [27]. When electrolysis operation is interrupted, the bipolar plate behaves like a galvanic cell. The discharge of electromotive force happens in the opposite direction to that of standard electrolysis current, thereby causing the anode and cathode to undergo reduction and oxidation, respectively, as shown in Fig. 1 (b) [28,29]. However, it is important to know that the change is not spontaneous. The electrodes undergo successive phases of transformation, each driven by an underlying force, as shown in Fig. 2. Initially, due to the presence of dissolved gases, the anode and cathode undergo oxygen reduction and hydrogen oxidation reactions, respectively. Later, the electrodes undergo changes to their original redox state, and finally, the hydrogen and oxygen production starts on the original anode and cathode, respectively.

One possible solution to tackle this problem is to employ polarization rectifiers in the balance of the plant; however, this increases the capital expenditures of the system and can lead to gas-purity issues due to crossover. If a polarization unit is not applied, the electrodes will be exposed to reverse currents, turning the cathode into anodes and vice versa [26]. Thus, it is essential to utilize electrodes that possess superior intrinsic activity and are inherently resistant to reverse currents. Despite the recent development of novel catalysts, better evaluation of catalysts is still necessary. Although PtRu has better activity than Pt in alkaline conditions, the stability of Ru in OER potential ranges is a significant concern; hence, more studies are essential to understand the catalyst sensitivity to possible reverse currents [30].

Next to better testing protocols for intermittent operation, there is also a need for improved characterization methods to evaluate different cell components to facilitate further development of AEMWE. The most accepted cell characterization practices in electrolysis are polarization curves and electrochemical impedance spectroscopy (EIS); however, these tests only measure full-cell performance. To further optimize system performance, it is crucial to understand the individual half-cell kinetics of the oxygen evolution reaction (OER) and hydrogen evolution reaction (HER). Reference electrodes can provide an opportunity to decouple individual electrode overpotentials.

The use of reference electrodes in flow cell systems remains relatively uncommon, with only a limited number of studies incorporating them. Traditionally, wire electrodes (e.g. platinum) have been employed, but they are relatively unstable and prone to drift. Consequently, they necessitate periodic calibration against some standard electrode to ensure accuracy and reliability. Certain studies in the realm of fuel cell and electrolyzer research have been experimented with an external reference electrode configuration [1,6,31–35]. In this configuration, the reference electrode is situated in a distinct compartment at room temperature. It is linked to the electrochemical cell through the utilization of an ionic bridge. Nevertheless, the external reference

electrode configuration comes with specific challenges. It is crucial to maintain pressure equilibrium between the reference electrode compartment and the electrochemical cell. Moreover, when the reactor operates at higher temperatures, adjustments must be made for thermal junction potentials in the measured reference potentials. Calculating these corrections necessitates understanding the heat transfer dynamics between the reactor and the reference electrode compartment [35,36].

A viable alternative to using an external reference electrode configuration involves implementing an internal reference electrode configuration. Dynamic Hydrogen Reference Electrode (DHRE) is a type of internal reference electrode configuration comprising two thin platinum wire electrodes (one hydrogen evolving electrode and one counter

electrode) which are placed close to the active electrode area, and a small microcurrent is passed through the Pt wires to maintain hydrogen coverage and establish equilibrium cell potential (few mV negative of 0 V vs RHE) [37–39]. To the best of our knowledge, this type of reference electrode has not yet been utilized in AEM systems.

This work focuses on uncovering the impact of reverse currents on electrode stability by using reference electrodes in an AEM electrolyzer. Using platinum wire DHRE and employing characterization techniques like electrochemical impedance spectroscopy and polarization curves, we investigate how the activity of bimetallic catalysts like PtRu and NiMo compares with traditional platinum catalysts in an alkaline environment during standard electrolysis operation and under start/stop

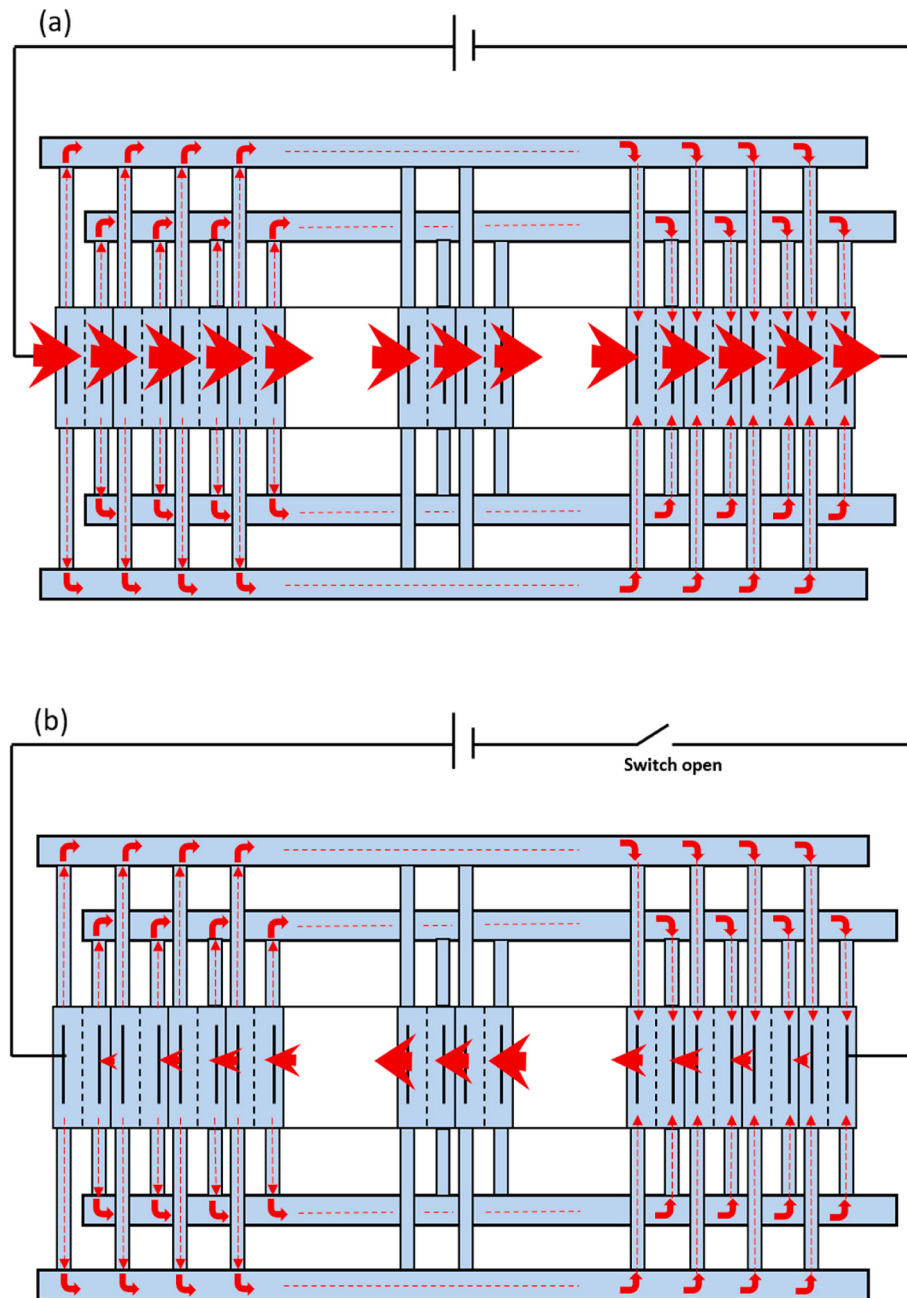


Fig. 1. General scheme of multi-cell electrolyzer stack operation with manifold assembly during (a) steady state and (b) shutdown conditions. Shunt currents (small red arrows) are typically symmetrical. They leave the cells in the positive half of the circuit, bypass the middle cells and reenter the negative half of the circuit [27]. During shutdown conditions, the bipolar plate behaves like a galvanic cell, and the electromotive force discharge is in the opposite direction. The circulation of conductive electrolytes from manifold assembly enables ionic current, thus forming a closed circuit. The cells in the centre experience the highest reverse currents, diminishing towards the periphery. (For interpretation of the references to colour in this figure legend, the reader is referred to the Web version of this article.)

conditions. Lastly, an effort is made to elucidate some challenges of employing pseudo-reference electrodes in flow cell systems.

2. Methods and materials

2.1. Chemicals and materials

Platinum on Vulcan XC-72R support (40 % Pt), Platinum ruthenium on high surface area ketjenblack EC-300J (50 % PtRu, Pt: Ru: 1:1) were purchased from the Fuel cell store. NiMo/C catalyst (50 wt%) was purchased from Pajarito powder. NiFe-LDH was synthesized by gelation-deflocculation using nickel chloride and iron chloride precursors according to the protocol from Koshikawa et al. [13]. Piperion membrane (60 µm) and ionomer solution (5 wt% in ethanol) were purchased from Versogen. Fiber-sintered nickel (Bekaert) with a thickness of 500 ± 10 µm, fiber diameter of 20 µm and a porosity of 66 % was used as PTL for both half-cells. Potassium hydroxide pellets ($\geq 85\%$ purity) were obtained from VWR chemicals, and 2-propanol was purchased from Sigma Aldrich.

2.2. Pretreatment of PTL and piperion membrane

Piperion membranes were obtained in dry form and are usually in bicarbonate form. Prior to electrolysis, the membrane needs to be converted to its OH⁻ form for optimal conductivity, for which the membranes were soaked in 1 M KOH overnight (for at least 24 h). All PTLs were precisely cut to a 5 cm² area for electrode fabrication. To improve the hydrophilicity of the nickel PTL and remove the surface hydroxide layer formed due to exposure to the atmosphere, all the PTLs were ultrasonicated in 1 M HCl for 10 min and washed with DI-water before employing them inside the flow cell [40].

2.3. Catalyst ink and electrode fabrication

For OER, NiFe-LDH nanoparticles were used as active electrocatalyst. For HER, Pt on Vulcan support, PtRu on Ketjenblack support or NiMo/C were used as catalysts. Catalyst inks consisting of 4 wt% solids and 96 wt% solvents were prepared. For every 100 mg of catalyst, 750 mg of DI water (18 MΩ cm), 3000 mg of 2-propanol (1:4 water/2 propanol), and 400 mg of Piperion ionomer (Ionomer: Catalyst = 0.2) were added. Then, the mixture was ultrasonicated in an ice bath for 90 min to ensure homogenous dispersion of the catalyst ink. All the cell configurations were developed using the catalyst-coated substrate (CCS) method [8]. The pre-cut, pretreated PTLs were used as the substrate upon which the catalyst inks were coated. The electrodes were prepared using a handheld airbrush spraying gun (Harder-Steenbeck). The airbrush was connected to a nitrogen line. The loaded inks were sprayed onto the nickel PTL using a meander-shaped spray pattern to ensure maximum

coverage and homogenous ink distribution. After every spray pass, the substrate was weighed and the spraying was continued until the desired loading ($2 \pm 0.2 \text{ mg cm}^{-2}$ for NiFe-LDH, $0.6 \pm 0.2 \text{ mg cm}^{-2}$ for Pt-based catalysts and $5 \pm 0.2 \text{ mg cm}^{-2}$ for NiMo/C catalyst) was reached. The substrate was placed on a hot plate (80 °C) during the coating process to ensure rapid evaporation of organic solvents from the ink.

2.4. Cell design and assembly

The performance of various cell configurations was evaluated in a commercially available flow cell of 5 cm² active area (quick CONNECT, Baltic fuel cells GmbH) with a pneumatic compression unit. Unlike traditional flow cells, the contact pressure can be controlled explicitly on the active area. Fig. 3 shows the various components of the flow cell along with a scheme that shows the integration of the reference electrode. The end plates consist of nickel flow fields (parallel channels) and gold-plated support plates for electrical contact. The membrane and the electrodes are sandwiched between two end plates and sealed with Viton gaskets. The reference electrode consists of an insulating foil with two platinum wire electrodes on one side. This reference electrode is placed in the cathode half-cell with the platinum wire tips touching the membrane outside the active area. It was ensured that the platinum tips did not touch the catalyst layer or the PTL surface. A small micro-current (20–30 µA) was passed through the platinum wires from an external current source to establish potential, which is very close to 0 V vs RHE. Positioning the DHRE in the cathode half-cell ensures a stable hydrogen pressure, facilitating the establishment of stable reference potential upon the HER over Pt wire. Positioning in the anode half-cell would probably lead to erroneous values due to the presence of oxygen.

2.5. Test bench

All the tests were performed using an in-house developed test bench, of which a schematic overview is shown in Fig. 4. In this work, a SP-150 potentiostat coupled to a 20 A booster (BioLogic) was used to apply the desired electrolytic current to the cell. A Proline P8 (LAUDA) thermostat was directly connected to the flow cell heating circuit for elevated temperature measurements. The test bench was designed to operate in separated circuit mode (no intermixing of anolyte and catholyte). The cell inlets and outlets were connected to two gas-liquid separators (1 L glass vessel). Supply of electrolyte (1 M KOH) to the flow cell from the gas-liquid separators was realized by two peristaltic pumps (Master Flex Easy-Load II) using PFA tubing (Swagelok 1/8th inch diameter). A small piece of flexible tubing (Puri-flex L/S 16) was used for the peristaltic pumps. Special peristaltic pump flangeless adapter sets (IDEX Corporation) were used to connect the flexible and PFA tubing. Four temperature sensors (type k) were connected to each of the inlet/outlet ports to monitor the temperature of the electrolyte. Nitrogen gas was purged

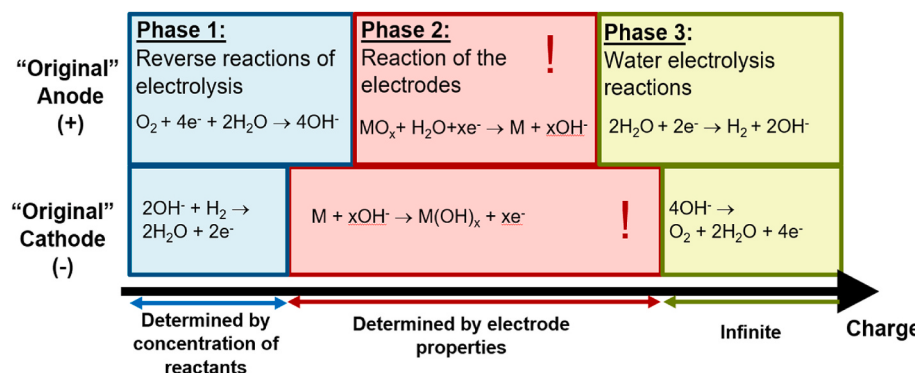


Fig. 2. Illustrative schematic depicting the successive changes the electrodes undergo in an electrolyzer during shutdown conditions, elucidating the underlying driving forces propelling each phase.

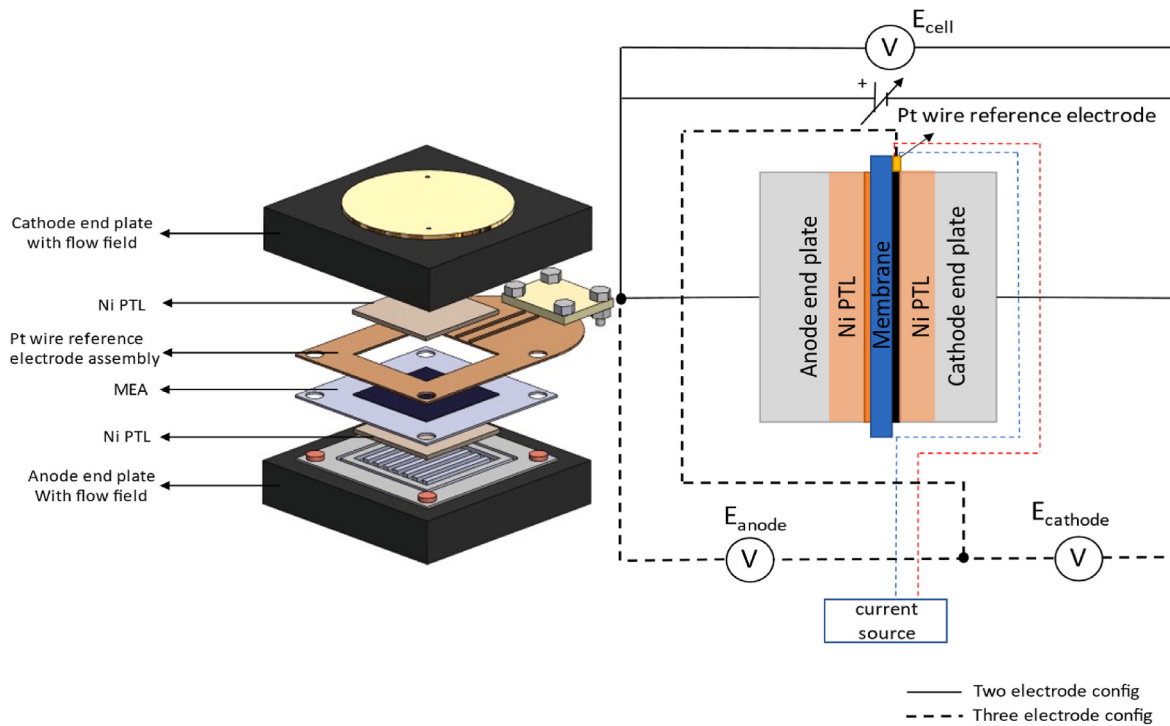


Fig. 3. Exploded view of 5 cm^2 flow cell depicting various components and positioning of the reference electrode assembly (left). Overview of different electrode connections (right) to potentiostat to obtain individual half-cell and total-cell potentials.

through both G/L separators.

2.6. Measurement protocol

This section details the measurement protocol used for all the cell configurations under investigation, as shown in Fig. S1. The cell is assembled in a humidified state. After assembly, it is inserted into the test bench as described in the previous section, and the cell is compressed to 1.5 MPa . Electrolyte circulation with a flow rate of 50 ml min^{-1} is used for both half cells, and the cell is heated up to $60\text{ }^\circ\text{C}$. Then, the cell conditioning process is used for newly assembled MEAs. The conditioning process helps hydrate the membrane and catalyst layer, as initial liquid saturation is insufficient for ideal ionic conduction. It also helps in creating ideal pathways for reactants and product transport [41]. Then, chronopotentiometry measurement is used to evaluate the cell response in step profile with current steps from 0.001 to 1.5 A cm^{-2} . EIS measurements were also conducted in the frequency range of 75 kHz – 100 mHz with 12 points per decade and 10 % amplitude of DC. After initial IV and EIS measurements, reference electrodes were employed to study individual cell contributions towards total cell potential. Half-cell HER and OER EIS measurements were performed to deconvolute the contributions of ohmic and charge transfer resistance. During half-cell EIS, the potentiostat simultaneously recorded working and counter-electrode potentials. Subsequently, polarities were reversed for 30 min at a current density of 0.03 A cm^{-2} (0.15 A) to mimic shutdown conditions. Later, the cell was reverted to standard conditions to study the possible effects of reverse currents on cell performance.

2.7. Post electrolysis measurements

X-ray photoelectron spectroscopy (XPS) and Inductively coupled plasma optical emission spectrometry (ICP-OES) measurements were carried out to elucidate the correlation between structural modifications, catalyst dissolution, and electrochemical performance pre- and post-application of reverse currents. XPS was measured on a Thermo Scientific instrument, equipped with a monochromated Al $\text{k}\alpha$ X-ray

source (1486.68 eV). Samples were prepared by affixing a small section of the electrode onto double sided carbon tape. High-resolution core level spectra were recorded with a pass energy of 50 eV ($500\text{ }\mu\text{m}$ spot size). All the associated peak fitting was performed using CasaXPS software, employing Shirley or Tougaard background subtraction methods.

Trace element analysis of the electrolyte was conducted utilizing iCAP PRO by Thermo-scientific. The samples were dissolved in 5 % w/v Nitric acid to ensure the dissolution of any suspended solids present in the electrolyte. The resulting solution was further diluted to total volume of 10 ml with $18\text{ M}\Omega$ DI water, ensuring that the total dissolved solids remained within the limit of 10 ppm . Calibration was carried out using standard solutions spanning concentrations from 0.001 to 10 ppm . The calibration curve derived from these standard solutions was subsequently employed to determine the concentration of various trace elements in the electrolyte.

3. Results and discussion

3.1. Effect of cathode catalyst

As described in the experimental section, AEM electrolyzers with electrodes of 5 cm^2 active area were investigated. NiFe-LDH coated on Ni PTL was used as the anode. As a cathode, three different catalysts were tested. Pt/Vulcan, PtRu/ketjenblack and NiMo/Vulcan spray coated on Ni PTL were employed as electrodes for hydrogen evolution. Hereafter, Pt/Vulcan, PtRu/Ketjenblack and NiMo/Vulcan will be referred to as Pt/C, PtRu/C and NiMo/C, respectively. Fig. 5 (a) shows the performance comparison of three MEAs with different cathode catalysts tested in 1 M KOH at $60\text{ }^\circ\text{C}$. Three independent measurements were conducted to demonstrate reproducibility, and the error bars depict the resulting coefficient of variation (standard deviation divided by mean) between these measurements.

The MEA using PtRu/C catalyst exhibits superior performance at 1.5 A cm^{-2} , achieving an operating potential of 1.77 V , in contrast to the MEAs utilizing Pt/C and NiMo/C catalyst at the same current density,

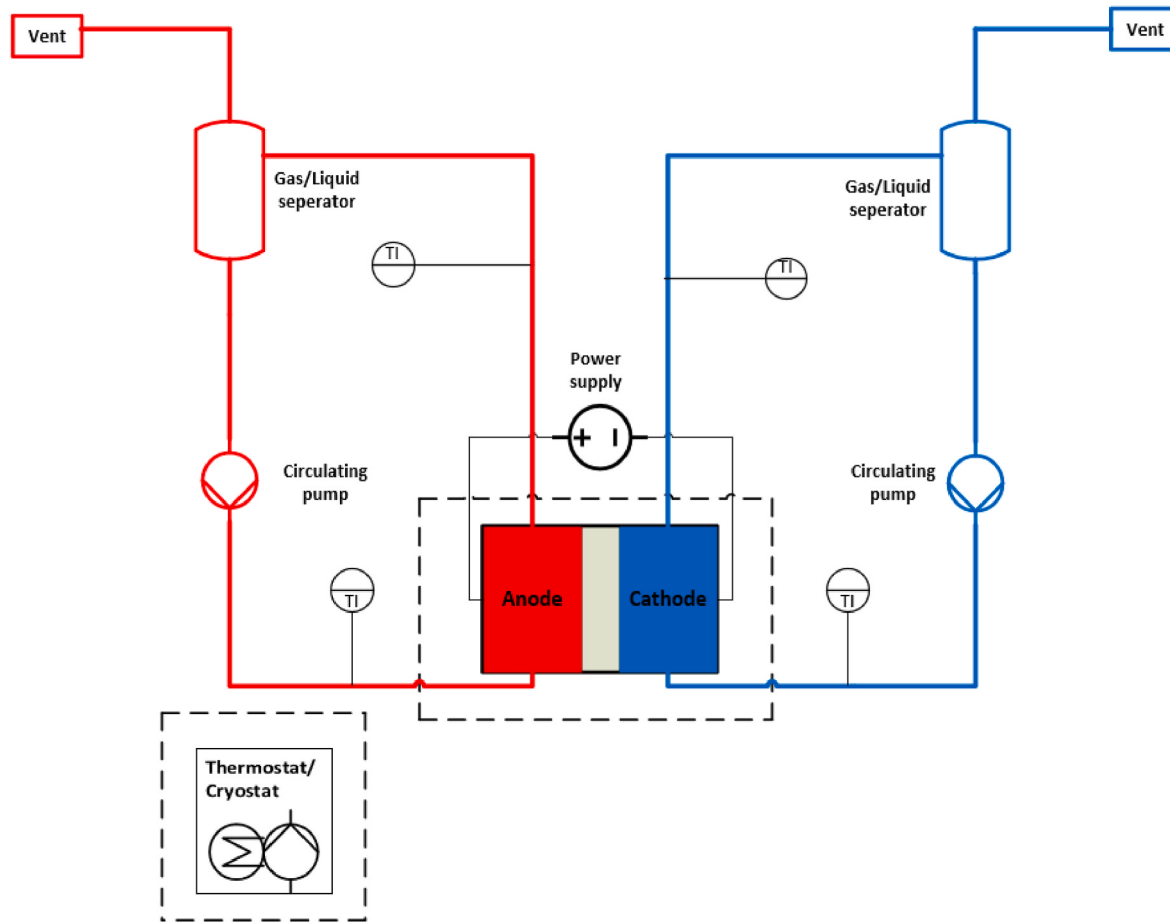


Fig. 4. Schematic overview of piping and instrumentation diagram (P&ID) showing various balance of plant components employed in the test bench consisting of two distinctive electrolytic circulation loops, anodic (red) and cathodic (blue). (For interpretation of the references to colour in this figure legend, the reader is referred to the Web version of this article.)

recording a higher operating voltage of 1.83 V and 1.97 V respectively. The better performance of the PtRu/C compared to Pt/C is attributed to the modification of the electronic properties of Pt by Ru due to ligand effects that can tailor the surface properties towards hydrogen absorption and optimize hydrogen binding energy [42–44]. Non-noble metal NiMo/C shows a significantly poorer performance compared to Pt-based catalysts.

To ascertain that the performance variation originates from the cathode catalyst, reference electrodes were employed to assess the individual electrode potentials within the kinetically dominant region (up to 0.2 A cm^{-2}), as shown in Fig. 5 (b). As the anode is the same in all three MEAs, the anodic electrode potential exhibits nearly identical values in all the measurements. In contrast, for the cathode, PtRu/C demonstrates a superior hydrogen evolution performance of approximately 50 mV compared to Pt/C and 90 mV compared to NiMo/C at 0.2 A cm^{-2} in line with the differences in cell potential observed at this current density. The accuracy of electrode potentials measured by platinum wire reference electrodes was verified by performing an identical experiment in a three-electrode setup under the same operating conditions (Fig. S2). The results indicate almost a perfect overlap at low current densities and a small difference of up to 20 mV at 0.2 A cm^{-2} . To further deconvolute the kinetic and ohmic contributions, EIS measurements were conducted. The accuracy of the measured plots was confirmed through the Kramers-Kronig transformation before any subsequent analysis using the LIN-KK software tool [45] (Fig. S3). Fig. 5 (c) shows the full-cell EIS spectrum of both MEAs at two different current densities. It possesses several distinctive features: first, a high-frequency inductive tail is followed by a small high-frequency semicircle (for a

more detailed view, see Fig. S4), and then a 45-degree line is followed by a semicircle indicative of kinetic dependence. Fig. 5 (c) shows that all MEAs have identical high-frequency resistances (HFR), and the charge transfer resistance (R_{CT}) decreases with an increase in current density, which generally agrees with the Tafel kinetics correlation [46]. Furthermore, the R_{CT} follows the trend of PtRu/C < Pt/C < NiMo/C at both current densities. The HER EIS plots in Fig. 5 (d) further show that the difference in R_{CT} can indeed be ascribed to the different cathode materials.

The Nyquist plots for all three systems show overlap at high frequencies. While there is no clear consensus on the origin of the high-frequency semicircle, Khataee et al. [40] hypothesized that the high-frequency semicircle is associated with interfacial contact resistances ($R_{contact}$) between different components arising from nickel hydroxide and nickel hydride formation. Lasia et al. [47] demonstrated that the high-frequency semicircle is overpotential independent and is only influenced by the electrode geometry and electrolyte resistivity. Jeon et al. [48] hypothesized that the high-frequency semicircle is possibly linked to the adsorbate capacitance arising due to different intermediate species on active sites of the catalyst during the OER. More focused studies are essential to understand which processes can be attributed to the high-frequency semicircle. The 45-degree line after the high-frequency semicircle appears to be linked with the ionic transmission resistance (R_{ionic}) associated with the transport of ions in the electrodes filled with electrolyte [49]. Notably, R_{ionic} is an inherent material property and doesn't change with increasing current densities (Fig. S4).

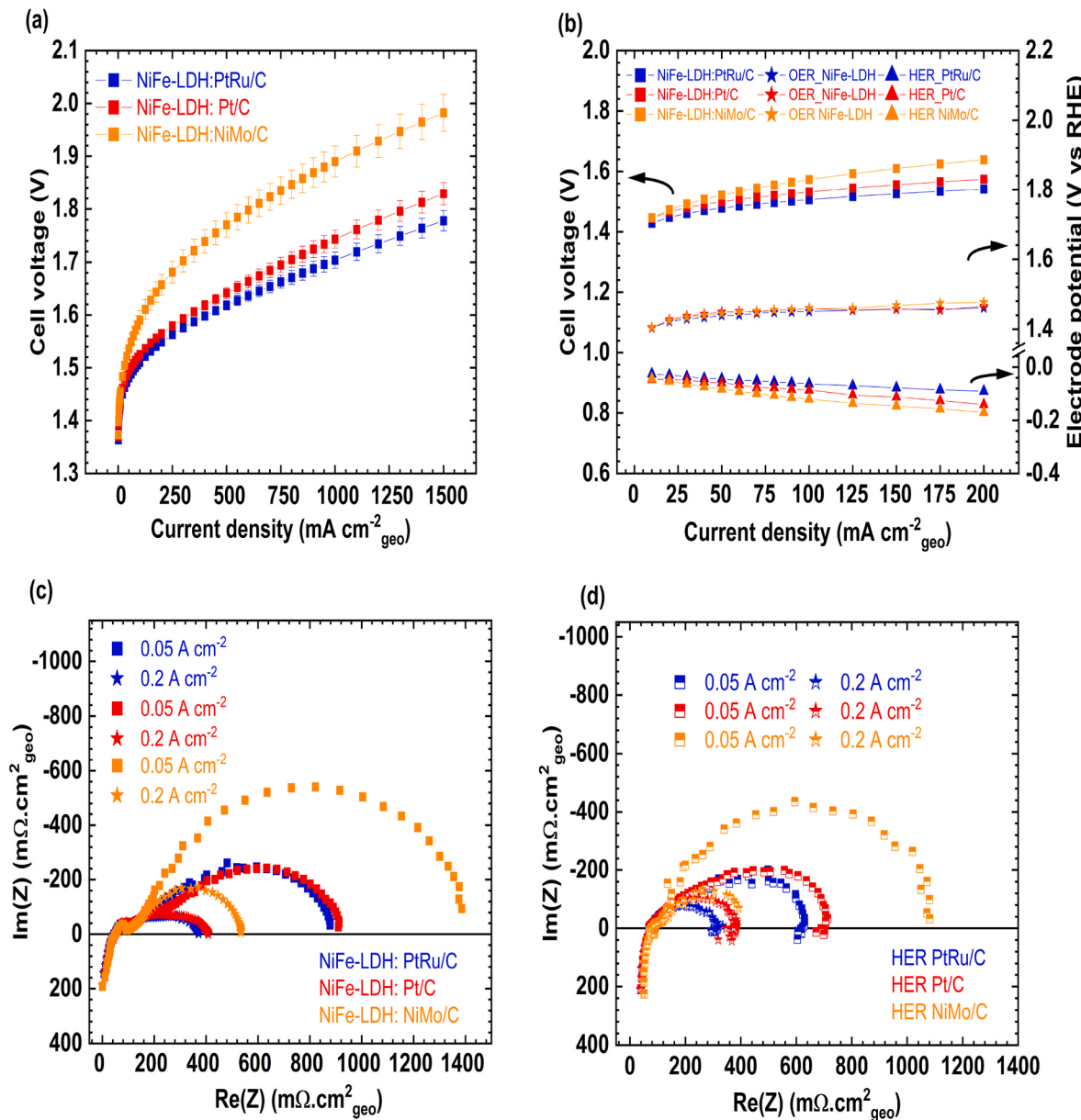


Fig. 5. Performance comparison of Pt/C, PtRu/C and NiMo/C cathode catalyst (a) Polarization curves for complete cell up to 1.5 A cm^{-2} . Reported values are the mean of three measurements, and the error bars represent the coefficient of variation (std deviation/mean) (b) Polarization curves for full cell, anode and cathode up to 0.2 A cm^{-2} as measured with reference electrodes. (c) Full cell EIS plots of three cell configurations at 0.05 and 0.2 A cm^{-2} . (d) Half-cell EIS showing cathodic performance comparison between Pt/C, PtRu/C and NiMo/C catalysts at 0.05 and 0.2 A cm^{-2} . All cell configurations were evaluated with Piperion membrane ($60 \mu\text{m}$) at 60°C using 1 M KOH and a flow rate of 50 ml min^{-1} (both half-cells). NiFe-LDH/20 % Piperion ionomer on Ni PTL was employed as anode for all measurements.

3.2. Effect of reverse currents

To evaluate the stability of the catalyst in a single cell, electrodes were reverse polarized to simulate reverse currents, a phenomenon commonly observed upon shutdown in bipolar multi-cell stacks with a conductive liquid electrolyte and joined inlet manifold. The actual duration and magnitude of reverse currents flowing in the stack depend on several parameters like the number of cells, manifold design, operating temperature, operating pressure, electrolyte flow during the shutdown and the cell's position in a stack [29]. In this study, polarities were reversed for 30 min with a current density of 0.03 A cm^{-2} (0.15 A : 2% of total current) to mimic the severe shutdown conditions that can especially affect the middle cells of electrolyzers. This is in line with the reverse currents that were previously reported for alkaline systems,

which are in the order of $0.1\text{--}1\%$ [29,50]. Yet, these reported values were for short stacks containing less than ten cells. For industrial-scale stacks with hundreds of cells, reverse currents are expected to be significantly higher, as reverse currents are related to shunt currents [29]. Shunt currents for alkaline systems can potentially reach tens of percent [51,52], depending on the cell and stack design. For an industrial alkaline electrolyzer, a value of 11.2% for the shunt currents has been reported [53]. One could argue that reverse currents in AEM are lower due to the use of 1 M KOH electrolyte compared to $6\text{--}7 \text{ M}$ used in alkaline systems, yet it should be noted that alkaline systems use special inlet designs to minimize shunt currents, which is not (yet) the case for AEM. Given the broad range of reported shunt currents in the literature, we adopted a conservative reverse current magnitude (2%) to evaluate the stability of different catalysts. A chronopotentiometric approach also

seems more representative of industrial conditions than the cyclic procedures that have been proposed [54]. The complete sequence of different steps employed in the study can be seen in the measurement protocol section (Fig. S1).

As the MEA incorporating PtRu/C demonstrated superior performance during normal electrolysis operation, our initial focus centered on examining the impact of reverse currents on this system, as shown in Fig. 6. The cell potential during the reverse current protocol can be seen in Fig. S5. The polarization curve results of the cell during standard operation (blue curve) and after application of reverse currents (magenta curve) are shown in Fig. 6 (a). The system shows considerable degradation (≈ 200 mV at 1.5 A cm^{-2}) in cell potential after reverse current application. To understand which electrode is responsible for the degradation, a reference electrode was used to obtain individual half-cell potentials, as shown in Fig. 6 (b). At 0.2 A cm^{-2} , the full-cell polarization curve shows ~ 55 mV of cell degradation. At the same current

density, the cathode shows degradation of around 50 mV, which indicates the cathode is more vulnerable to reverse currents than the anode, which remains relatively stable. EIS measurements were also done to deconvolute different overpotentials in the system, as shown in Fig. 6 (c). Furthermore, HER impedance plots in Fig. 6 (d) demonstrate a comparable rise in R_{CT} akin to that observed in the full-cell EIS, suggesting the loss in performance likely originates from the cathode half-cell. The OER EIS plots showed no noticeable deviation before and after reverse currents (Fig. S6), indicating the relative stability of the OER catalyst.

The degradation of the cathode can probably be ascribed to deactivation or dissolution of the ruthenium. During the HER reaction, Ru in alkaline media can form hydroxylated species (Ru(OH)_x). When the catalyst is subjected to oxidative currents after HER, these hydroxylated species form soluble ruthenates (RuO_4^{2-}) and possibly other higher oxidation state compounds that undergo dissolution, leading to a loss of

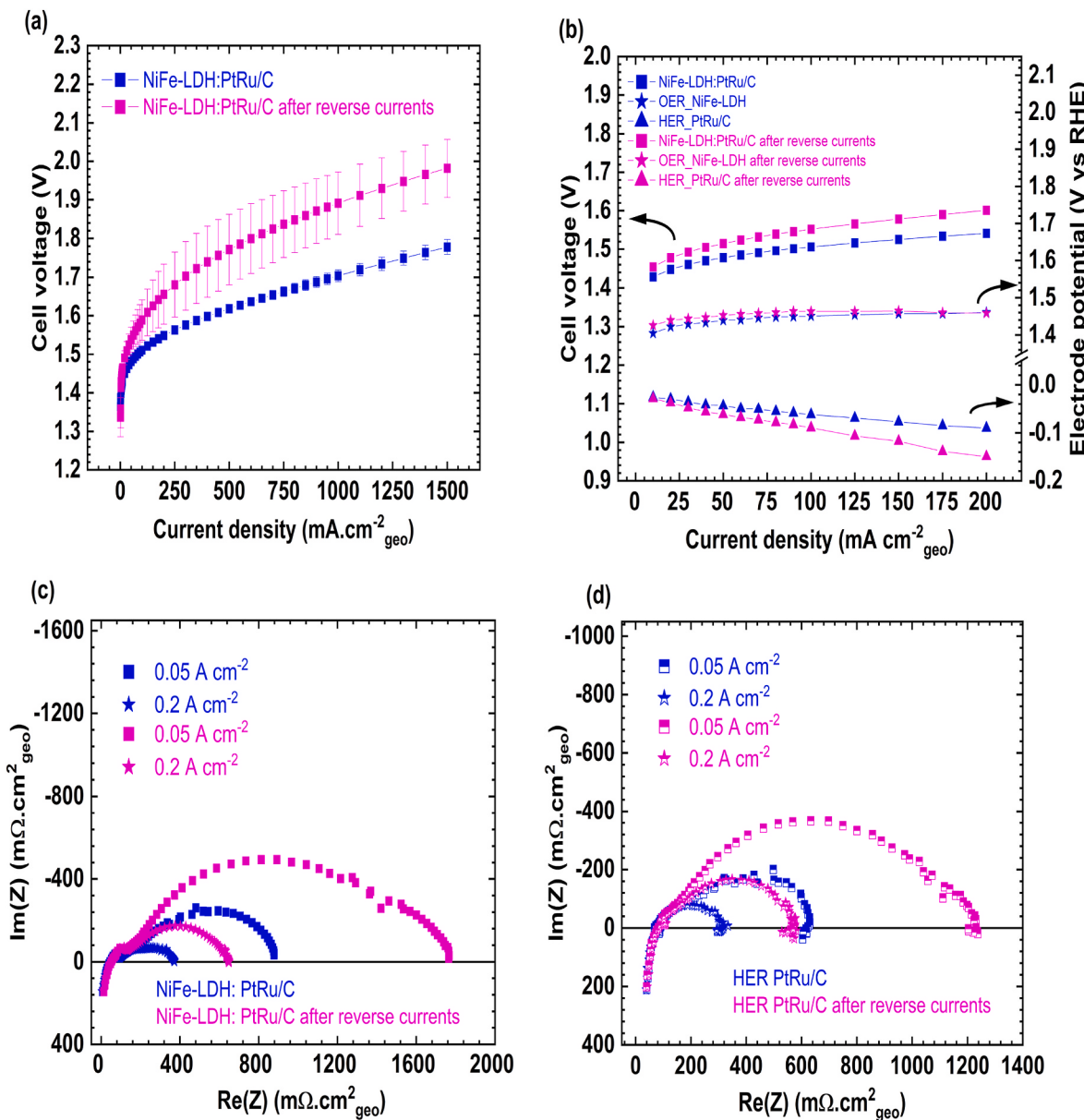


Fig. 6. Performance comparison of PtRu/C before and after application of reverse currents. (a) Polarization curve results for complete cell up to 1.5 A cm^{-2} . Reported values are the mean of three measurements, and the error bars represent the coefficient of variation (std deviation/mean) (b) Polarization curves for full cell, anode and cathode up to 0.2 A cm^{-2} as measured with reference electrodes. (c) Full cell EIS of the system at 0.05 and 0.2 A cm^{-2} showing apparent performance degradation after reverse currents. (d) HER EIS indicates the change in cathode performance. The cell was evaluated with Piperion membrane ($60 \mu\text{m}$) at 60°C using 1 M KOH and a flow rate of 50 ml min^{-1} (both half-cells). NiFe-LDH/20 % Piperion ionomer on Ni PTL was employed as the anode.

active sites and activity of the catalyst [30]. It is evident from Fig. 6 (c) that the ohmic resistance of the system before and after reverse currents remained identical, while charge transfer resistance saw a significant increase, which could be explained by multiple hypotheses.

Ruthenium dissolution in the form of ruthenates could result in the restructuring of surrounding Pt atoms, leading to HER with a different mechanism (higher Tafel slope). Moreover, carbon experiences thermodynamic instability when exposed to cell potentials higher than 0.207 V vs RHE [55]. Electrochemical oxidation of carbon can lead to CO₂, CO and bicarbonate anions forming in alkaline media, typically leading to loss of electrical conductivity, leading to detachment of active sites and thereby reducing electrochemical surface area [56]. Recent corrosion studies of standard carbon substrates like Ketjen, Vulcan and graphite in alkaline media showed CO evolution above 1 V vs RHE, indicating carbon oxidation [56]. Although there are extensive studies elucidating the potential-dependent redox reactions of Ru and RuO₂ corrosion in acidic media [57–59], there remains a need for further

investigation to comprehend the dissolution mechanisms in an alkaline environment and assess whether the Pt: Ru alloying ratio plays any role in mitigating corrosion.

The measured XPS results are presented in Fig. S7, which includes high-resolution spectra of C1s, Pt 4f and Ru3p at various stages of operation. The C1s spectra (Fig. S7 a,d,g) overlap with the Ru 3d spectra, displaying multiple distinguishable peaks. Metallic ruthenium states are distinctly visible for pristine electrodes and steady-state electrolysis. However, these states disappear after the application of reverse currents (Figs. S7 and g). Similarly, the Pt4f spectra exhibit significant changes post-application of reverse currents, with a notable reduction in the contribution of metallic Pt and a substantial increase in PtO_x contributions (Figs. S7 and h). The Ru3p spectra after application of reverse currents show no discernible peaks suitable for fitting, indicating substantial dissolution of ruthenium particles. To further quantify the dissolution, ICP-OES measurements were conducted, with results presented in Table S1. Following the application of reverse currents, the

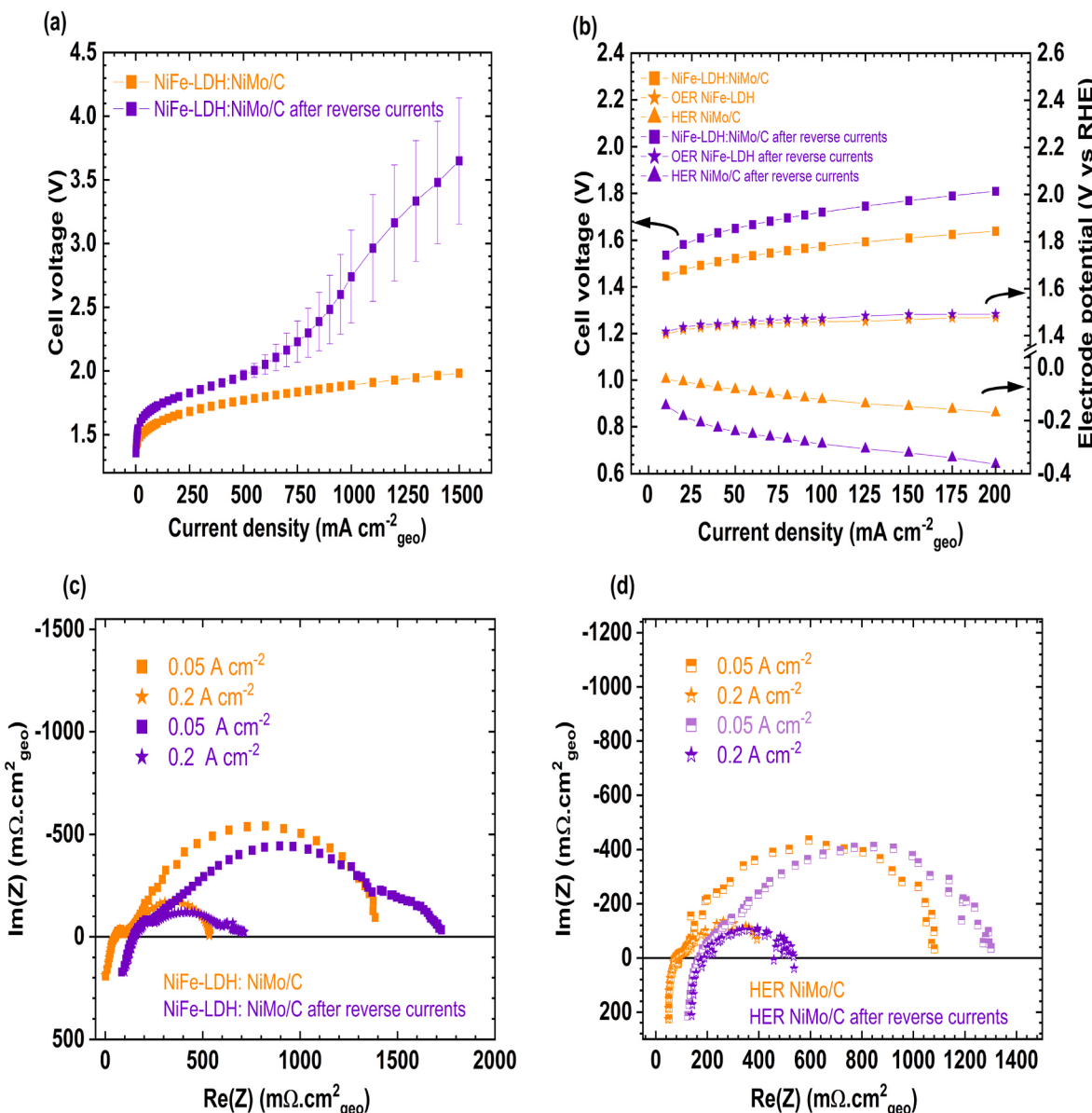


Fig. 7. Performance comparison of NiMo/C catalyst before and after application of reverse currents. (a) Polarization curves for complete cell up to 1.5 A cm^{-2} . (b) Polarization curves for full cell, anode and the cathode up to 0.2 A cm^{-2} as measured with reference electrodes. (c) Full cell EIS at 0.05 and 0.2 A cm^{-2} . (d) HER EIS contribution of NiMo/C at 0.05 and 0.2 A cm^{-2} . The cell was evaluated with Piperion membrane ($60 \mu\text{m}$) at 60°C using 1 M KOH and a flow rate of 50 ml min^{-1} (both half-cells). NiFe-LDH/20 % Piperion ionomer on Ni PTL was employed as the anode.

ruthenium concentration in the electrolyte was measured at 2.23 ppm. This corresponds to an approximate 36 % of initial ruthenium catalyst loading based on an electrolyte amount of 40 mL.

Since the PtRu/C catalyst suffered severe degradation under the influence of reverse currents, the next logical step was to investigate Pt/C under reverse currents. Similar to PtRu/C, even the Pt/C catalyst showed a drop in performance, but the degradation was significantly lower (≈ 50 mV at 1.5 A cm^{-2}). The polarization curve and EIS results of Pt/C before and after reverse currents are depicted in Fig. S8. The observed lower degradation can possibly be explained by the fact that at higher anodic potentials, in contrast to Ru, the Pourbaix diagram of Pt shows the formation of two transition oxidation states, namely PtO and PtO₂ [60]. The higher stability of these oxide layers and associated kinetic barriers can be a possible explanation for lower cell degradation when compared to the PtRu system [61,62].

The degradation of the NiMo/C is significantly worse than for the noble metal-based systems. Fig. 7 (a) shows the polarization curve behavior of the NiMo/C system before and after the application of reverse currents. Unlike the MEA with platinum-based catalysts, this system shows an extreme cell potential increase ($\approx +1.7 \text{ V}$ at 1.5 A cm^{-2}) after reverse current application. Although the cell potential is already significantly higher at low current densities, the cell potential especially increases dramatically after 0.75 A cm^{-2} .

Individual electrode potentials obtained with reference electrodes (Fig. 7 (b)) clearly show cathode degradation, while there is no notable rise in the potential at the anode. Full cell EIS results in Fig. 7 (c) indicate a 150 % increase in the high-frequency ohmic resistance along with the emergence of a second semicircle at lower frequencies after reverse current application, likely indicating mass transfer limitations [63,64]. We are not sure about the exact origin of the increase of the HFR, but we believe ionomer degradation is a possible scenario under higher oxidative potentials [65,66]. Moreover, the loss of active sites (shown by XPS results, Fig. S9) can lead to restructuring of catalyst layer and thereby disrupting the optimal pathways for ion conduction. HER EIS of NiMo/C in Fig. 7 (d) shows a similar increase in charge transfer and ohmic resistances, indicating that the cathode is driving the cell degradation. Our results show that although NiMo/C exhibits decent HER activity (1.9 V @ 1 A cm^{-2}) for a non-PGM catalyst [67], its stability is an issue, especially under intermittent conditions. Several studies indicate that Mo leaches out at open circuit potential (OCP) and at anodic potentials [68–70]. Wang et al. calculated the Pourbaix diagram of NiMo, illustrating various stable phases existing at specific pH and potential ranges. They further demonstrated that Ni₃Mo decomposes to form MoO₂ around OCP, while MoO₄²⁻ (molybdates) and Ni(OH)₂ are formed at potentials greater than 0 V vs RHE [70].

XPS measurement results for NiMo are presented in Fig. S9, which includes high-resolution spectra of C1s, Mo3d and Ni2p. The peak fitting of the pristine electrode for Mo3d reveals Mo oxidation states ranging from Mo⁰ to Mo⁺⁶, while under steady state operation, Mo⁰ and Mo⁺⁵ predominate. However, post application of reverse currents, the spectra becomes indistinct, indicating catalyst dissolution similar to PtRu XPS results. ICP-OES measurements were conducted to quantify this dissolution, with results tabulated in Table S1. Significant Mo concentrations were detected after steady-state electrolysis (3.64 ppm) and following reverse current protocol (8.80 ppm). This corresponds to approximately 37 % and 88 % molybdenum loss from the initial catalyst loading respectively.

3.3. Challenges of employing pseudo-reference electrodes

While we have demonstrated the functionality of pseudo-reference electrodes in the preceding sections, there are certain challenges associated with their use. One common problem is that the reference potential measured by these pseudo-reference electrodes drifts with time. This could be due to significant surface changes on these wire electrodes during the experiment; hence, the reference potential could change due

to a reaction with impurities in the electrolyte or the deposition of oxide compounds onto the metal surface [71]. Another prevalent issue is the stability of these pseudo-reference electrodes at higher current density operation. At these current densities, the reference potential drifts significantly, thereby rendering the measurement above 0.2 A cm^{-2} challenging. Hydrogen supersaturation could possibly play a role in the instability of reference electrodes. With increasing current densities, the concentration of dissolved hydrogen increases, leading to rising local supersaturation [72]. This could disturb the equilibrium conditions around the reference electrodes, leading to a drift in potentials. Based on the Nernst equation, a rise in hydrogen supersaturation by 1 bar corresponds to an upward shift of the reference potential by around 10 mV.

Positioning of these reference electrodes with respect to active electrodes could also have a significant impact on impedance measurements. Fig. 8 shows a typical example of this study's impedance spectra obtained for full-cell and individual electrodes. Ideally, adding resistances obtained from two half-cell Nyquist plots should match with those obtained in full-cell impedance plots. While that is indeed the case, the HFR at the cathode surpasses that of the full cell and the HFR from the anodic half-cell was shifted to the negative x-axis. This could possibly be explained by asymmetrical potential profiles along the membrane surface due to the misalignment of electrodes [73]. Through finite element calculations, S B Adler [74] demonstrated that the full cell impedance is independent of electrode misalignment. Nonetheless, substantial inaccuracies in half-cell impedances can occur due to alignment errors, potentially resulting in misinterpretations of the physical processes influencing electrode behavior. This effect has a direct dependence on the membrane thickness. For thin membranes such as the one used in this study, any small misalignment is already huge relative to the membrane thickness, thereby possibly resulting in measurement errors [73]. In summation, we have utilized a reference electrode concept that provides reasonable results, albeit with certain limitations that need to be accounted for during data analysis.

4. Conclusions

In summary, we incorporated an in-situ Pt-wire pseudo-reference electrode assembly inside AEMWE to understand the activity and stability of individual electrodes. Different PGM and non-PGM-based

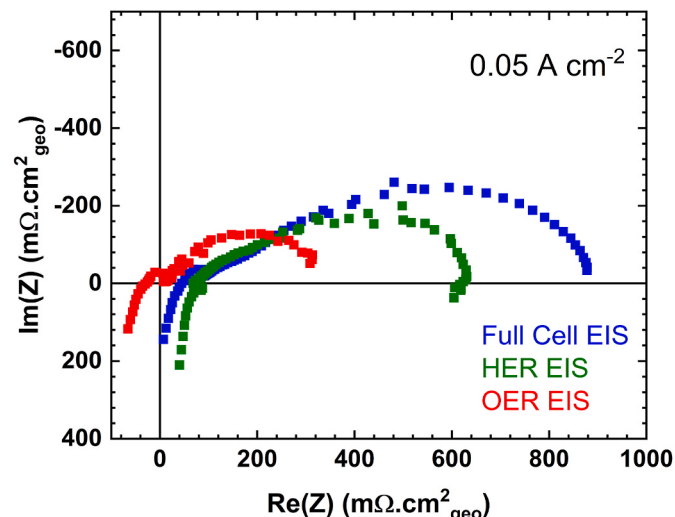


Fig. 8. Comparison of full cell and individual electrode Nyquist plots obtained from reference electrodes at a current density of 0.05 A cm^{-2} . Clear deviation in HFR among the three plots can be observed, which could be attributed to possible misalignment of electrodes. Experimental conditions: 1 M KOH , 60°C , 50 ml min^{-1} flow rate, Piperion ($60 \mu\text{m}$) membrane, PtRu/C cathode catalyst (0.6 mg cm^{-2} loading) and NiFe-LDH anode catalyst (2 mg cm^{-2} loading) was employed.

cathode catalysts were tested. Under normal operating conditions, the observed catalyst activity displayed the trend in the order of PtRu/C > Pt/C > NiMo/C.

The stability of individual electrodes to frequent shutdowns was evaluated by applying reverse currents. Results show that all cathode materials are susceptible to these reverse currents, while the anode remains relatively stable. The observed degradation in MEA performance displayed the trend in order NiMo/C > PtRu/C > Pt/C, with the degradation being especially detrimental to the NiMo/C.

Future strategies for catalyst development must account for the potential impact of reverse currents, and therefore, reverse currents should become part of accelerated stress testing protocols. In this study, we employed a reverse current protocol to show the potential detrimental effect of reverse currents. Yet, more exhaustive investigations are necessary to properly assess the height of the reverse currents upon electrolyzer shutdown. This requires both modeling as well as testing and validation within an operational stack.

The findings from this study demonstrate the functionality of Pt-wire reference electrodes. Their relatively simple construction and ease of use make them ideally suitable for integration in multi-cell stacks. However, more tests are essential to confirm their viability in high-pressure and high-temperature environments.

CRediT authorship contribution statement

Naveen Guruprasad: Writing – review & editing, Writing – original draft, Visualization, Software, Methodology, Investigation, Formal analysis, Data curation, Conceptualization. **John van der Schaaf:** Writing – review & editing, Supervision, Project administration, Conceptualization. **Matheus T. de Groot:** Writing – review & editing, Visualization, Supervision, Resources, Project administration, Methodology, Funding acquisition, Conceptualization.

Declaration of competing interest

The authors declare that they have no known competing financial interests or personal relationships that could have appeared to influence the work reported in this paper.

Data availability

All the raw data associated with results shown in the main text and the supplementary information has been deposited with Mendeley datasets and is publicly available as of the date of publication under <https://data.mendeley.com/datasets/3nn8x5hztk/1>

Acknowledgements

This research received funding from the Dutch Research Council (NWO) in the framework of the Reversible Large Scale Energy Storage [RELEASE] Project (Grant number: 17621). The authors further acknowledge Adarsh Patil and Anouk W.N de Leeuw den Bouter for their assistance in synthesizing NiFe-LDH nanoparticles and measuring XPS spectra of cathode catalysts.

Appendix A. Supplementary data

Supplementary data to this article can be found online at <https://doi.org/10.1016/j.jpowsour.2024.234877>.

References

- [1] A.Y. Paid, S. Sunde, Anion exchange membrane water electrolysis from catalyst design to the membrane electrode assembly, in: *Energy Technology*, vol. 10, John Wiley and Sons Inc, 2022.
- [2] N. Du, C. Roy, R. Peach, M. Turnbull, S. Thiele, C. Bock, Anion-Exchange Membrane Water Electrolyzers, vol. 122, *Chemical Reviews*. American Chemical Society, 2022, pp. 11830–11895.
- [3] G. Tjarks, J. Mergel, D. Stolten, Dynamic operation of electrolyzers - systems design and operating strategies, in: *Hydrogen Science and Engineering: Materials, Processes, Systems and Technology*, Wiley-VCH Verlag, 2016, pp. 309–329.
- [4] P. Haug, B. Kreitz, M. Koj, T. Turek, Process modelling of an alkaline water electrolyzer, *Int. J. Hydrogen Energy* 42 (24) (2017 Jun 15) 15689–15707.
- [5] P. Haug, M. Koj, T. Turek, Influence of process conditions on gas purity in alkaline water electrolysis, *Int. J. Hydrogen Energy* 42 (15) (2017 Apr 13) 9406–9418.
- [6] A.W. Tricker, J.K. Lee, J.R. Shin, N. Danilovic, A.Z. Weber, X. Peng, Design and operating principles for high-performing anion exchange membrane water electrolyzers, *J. Power Sources* 567 (2023 May) 232967.
- [7] H. Ito, N. Kawaguchi, S. Someya, T. Munakata, Pressurized operation of anion exchange membrane water electrolysis, *Electrochim. Acta* 297 (2019 Feb 20) 188–196.
- [8] Q. Xu, L. Zhang, J. Zhang, J. Wang, Y. Hu, H. Jiang, et al., Anion exchange membrane water electrolyzer: electrode design, lab-scaled testing system and performance evaluation, *Inside Energy* 4 (2022). Elsevier B.V.
- [9] K.F.L. Hagesteijn, S. Jiang, B.P. Ladewig, A review of the synthesis and characterization of anion exchange membranes, *J. Mater. Sci.* 53 (2018) 11131–11150. Springer New York LLC.
- [10] Y. Yang, P. Li, X. Zheng, W. Sun, S.X. Dou, T. Ma, et al., Anion-exchange membrane water electrolyzers and fuel cells, *Chem. Soc. Rev.* 51 (23) (2022) 9620–9693.
- [11] J. Zhang, L. Yu, Y. Chen, X.F. Lu, S. Gao, X.W. Lou, Designed Formation of double-shelled Ni–Fe layered-double-hydroxide nanocages for efficient oxygen evolution reaction, *Adv. Mater.* 32 (16) (2020 Apr 1).
- [12] W. Jiang, A.Y. Paid, B.F. Gomes, I. Galkina, L. Xia, C.M.S. Lobo, et al., Composition-dependent morphology, structure, and catalytical performance of nickel–iron layered double hydroxide as highly-efficient and stable anode catalyst in anion exchange membrane water electrolysis, *Adv. Funct. Mater.* 32 (38) (2022 Sep 1).
- [13] H. Koshikawa, H. Murase, T. Hayashi, K. Nakajima, H. Mashiko, S. Shiraishi, et al., Single nanometer-sized NiFe-layered double hydroxides as anode catalyst in anion exchange membrane water electrolysis cell with energy conversion efficiency of 74.7% at 1.0 A cm⁻², *ACS Catal.* 10 (3) (2020 Feb 7) 1886–1893.
- [14] X. Cui, P. Ren, D. Deng, J. Deng, X. Bao, Single layer graphene encapsulating non-precious metals as high-performance electrocatalysts for water oxidation, *Energy Environ. Sci.* 9 (1) (2016 Jan 1) 123–129.
- [15] L. Wu, L. Yu, X. Xiao, F. Zhang, S. Song, S. Chen, et al., Recent Advances in Self-Supported Layered Double Hydroxides for Oxygen Evolution Reaction, 2020 Jan; 2020. Research.
- [16] C.C.L. McCrory, S. Jung, I.M. Ferrer, S.M. Chatman, J.C. Peters, T.F. Jaramillo, Benchmarking hydrogen evolving reaction and oxygen evolving reaction electrocatalysts for solar water splitting devices, *J. Am. Chem. Soc.* 137 (13) (2015 Apr 8) 4347–4357.
- [17] Diana Bauer, Ruby Nguyen, Braeton Smith, US Department of Energy, Critical Materials Assessment - July, 2023 [Internet], Available from: https://www.energy.gov/sites/default/files/2023-07/doe-critical-material-assessment_07312023.pdf.
- [18] J. Zheng, W. Sheng, Z. Zhuang, B. Xu, Y. Yan, Universal dependence of hydrogen oxidation and evolution reaction activity of platinum-group metals on pH and hydrogen binding energy, *Sci. Adv.* 2 (3) (2016 Mar 1).
- [19] W. Sheng, H.A. Gasteiger, Y. Shao-Horn, Hydrogen oxidation and evolution reaction kinetics on platinum: acid vs alkaline electrolytes, *J. Electrochem. Soc.* 157 (11) (2010) B1529.
- [20] L. Li, G. Zhang, B. Wang, T. Yang, S. Yang, Electrochemical formation of PtRu bimetallic nanoparticles for highly efficient and pH-universal hydrogen evolution reaction, *J. Mater. Chem. A Mater.* 8 (4) (2020) 2090–2098.
- [21] D. Li, E.J. Park, W. Zhu, Q. Shi, Y. Zhou, H. Tian, et al., Highly quaternized polystyrene ionomers for high performance anion exchange membrane water electrolyzers, *Nat. Energy* 5 (5) (2020 May 1) 378–385.
- [22] J. Liu, Z. Kang, D. Li, M. Pak, S.M. Alia, C. Fujimoto, et al., Elucidating the role of hydroxide electrolyte on anion-exchange-membrane water electrolyzer performance, *J. Electrochem. Soc.* 168 (5) (2021 May 1) 054522.
- [23] I. Matanovic, Y.S. Kim, Electrochemical phenyl oxidation: a limiting factor of oxygen evolution reaction in water electrolysis, *Curr. Opin. Electrochem.* 38 (2023). Elsevier B.V.
- [24] D. Li, I. Matanovic, A.S. Lee, E.J. Park, C. Fujimoto, H.T. Chung, et al., Phenyl oxidation impacts the durability of alkaline membrane water electrolyzer, *ACS Appl. Mater. Interfaces* 11 (10) (2019 Mar 13) 9696–9701.
- [25] R. Subbaraman, D. Tripkovic, K.C. Chang, D. Strmcnik, A.P. Paulikas, P. Hirunsit, et al., Trends in activity for the water electrolyser reactions on 3d M(Ni,Co,Fe,Mn) hydr(oxy)oxide catalysts, *Nat. Mater.* 11 (6) (2012) 550–557.
- [26] J. Zhang, T. Wang, P. Liu, Z. Liao, S. Liu, X. Zhuang, et al., Efficient hydrogen production on MoNi 4 electrocatalysts with fast water dissociation kinetics, *Nat. Commun.* 17 (2017 May) 8.
- [27] T. O'Brien, T.V. Bommaraju, Hine Fumio, *Handoook of Chlor-Alkali Technology*, Springer, 2005, p. 1582.
- [28] Y. Kim, S.M. Jung, K.S. Kim, H.Y. Kim, J. Kwon, J. Lee, et al., Cathodic protection system against a reverse-current after shut-down in zero-gap alkaline water electrolysis, *JACS Au* 2 (11) (2022 Nov 28) 2491–2500.
- [29] A. Abdel Haleem, J. Huyan, K. Nagasawa, Y. Kuroda, Y. Nishiki, A. Kato, et al., Effects of operation and shutdown parameters and electrode materials on the reverse current phenomenon in alkaline water analyzers, *J. Power Sources* 535 (2022 Jul 1) 231454.

- [30] S. Holmin, L.Å. Näslund, Á.S. Ingason, J. Rosen, E. Zimmerman, Corrosion of ruthenium dioxide based cathodes in alkaline medium caused by reverse currents, *Electrochim. Acta* 146 (2014 Nov 10) 30–36.
- [31] Q. Xu, S.Z. Oener, G. Lindquist, H. Jiang, C. Li, S.W. Boettcher, Integrated reference electrodes in anion-exchange-membrane electrolyzers: impact of stainless-steel gas-diffusion layers and internal mechanical pressure, *ACS Energy Lett.* 6 (2) (2021 Feb 12) 305–312.
- [32] J. Dodwell, M. Maier, J. Majasian, R. Jervis, L. Castanheira, P. Shearing, G. Hinds, D.J.L. Brett, Open-circuit dissolution of platinum from the cathode in polymer electrolyte membrane water electrolyzers, *Journal of Power Sources*, Volume 498, 2021, 229937.
- [33] E. Brightman, J. Dodwell, N. Van Dijk, G. Hinds, In situ characterisation of PEM water electrolyzers using a novel reference electrode, *Electrochim. Commun.* 52 (2015 Mar 1) 1–4.
- [34] L.V. Bühl, S. Bullerdiek, P. Trinke, B. Bensmann, A.L.E.R. Deutscher, P. Behrens, et al., Application and analysis of a salt bridge reference electrode setup for PEM water electrolysis: towards an extended voltage loss breakdown, *J. Electrochem. Soc.* 169 (12) (2022 Dec 1) 124513.
- [35] P. Leua, C. Chatzichristodoulou, Reversible hydrogen and Pd hydride reference electrodes with electrochemically supplied H₂ for high temperature and pressure electrochemistry, *J. Electrochim. Soc.* 169 (5) (2022 May 1) 054534.
- [36] N. Uwitonze, W. Chen, D. Zhou, Z. He, Y.X. Chen, The determination of thermal junction potential difference, *Sci. China Chem.* 61 (8) (2018 Aug 1) 1020–1024.
- [37] A. Hartig-Weiß, M. Bernt, A. Siebel, H.A. Gasteiger, A platinum micro-reference electrode for impedance measurements in a PEM water electrolysis cell, *J. Electrochim. Soc.* 168 (11) (2021 Nov 1) 114511.
- [38] Z. Siroma, R. Kakitsubo, N. Fujiwara, T. Ioroi, S.I. Yamazaki, K. Yasuda, Compact dynamic hydrogen electrode unit as a reference electrode for PEMFCs, *J. Power Sources* 156 (2) (2006 Jun 1) 284–287.
- [39] G. Li, P.G. Pickup, Measurement of single electrode potentials and impedances in hydrogen and direct methanol PEM fuel cells, *Electrochim. Acta* 49 (24) (2004 Sep 30) 4119–4126.
- [40] A. Khataee, A. Shirole, P. Jannasch, A. Krüger, A. Cornell, Anion exchange membrane water electrolysis using AemionTM membranes and nickel electrodes, *J Mater Chem A Mater* 10 (30) (2022 Jul 5) 16061–16070.
- [41] W. Wang, K. Li, L. Ding, S. Yu, Z. Xie, D.A. Cullen, et al., Exploring the impacts of conditioning on proton exchange membrane electrolyzers by in situ visualization and electrochemistry characterization, *ACS Appl. Mater. Interfaces* 14 (7) (2022 Feb 23) 9002–9012.
- [42] X. Tian, P. Zhao, W. Sheng, Hydrogen evolution and oxidation: mechanistic studies and material advances, in: Advanced Materials, vol. 31, Wiley-VCH Verlag, 2019.
- [43] Y. Wang, G. Wang, G. Li, B. Huang, J. Pan, Q. Liu, et al., Pt-Ru catalyzed hydrogen oxidation in alkaline media: oxophilic effect or electronic effect? *Energy Environ. Sci.* 8 (1) (2015 Jan 1) 177–181.
- [44] J.N. Schwämmlein, B.M. Stühmeier, K. Wagenbauer, H. Dietz, V. Tileli, H. A. Gasteiger, et al., Origin of superior HOR/HER activity of bimetallic Pt-Ru catalysts in alkaline media identified via Ru@Pt core-shell nanoparticles, *J. Electrochim. Soc.* 165 (5) (2018) H229–H239.
- [45] M. Schönleber, Kramers-Kronig Validity Test Lin-KK for Impedance Spectra, (n.d.). [Internet]. Available from: <https://www.iam.kit.edu/wet/english/Lin-KK.php>.
- [46] C. Rozain, P. Millet, Electrochemical characterization of polymer electrolyte membrane water electrolysis cells, *Electrochim. Acta* 131 (2014 Jun 10) 160–167.
- [47] C. Hitz, A. Lasia, Experimental study and modeling of impedance of the her on porous Ni electrodes, *Journal of Electroanalytical Chemistry* 500 (1–2) (2001) 213–222.
- [48] S.S. Jeon, P.W. Kang, M. Klingenhof, H. Lee, F. Dionigi, P. Strasser, Active surface area and intrinsic catalytic oxygen evolution reactivity of NiFe LDH at reactive electrode potentials using capacitances, *ACS Catal.* 13 (2) (2023 Jan 20) 1186–1196.
- [49] Y. Guo, X. Li, Q. Qin, Z. Wang, H. Guo, J. Wang, et al., Determination of the tortuosity and contact resistances in thick graphite anodes via electrochemical impedance spectroscopy, *J. Power Sources* 569 (2023) Jun 15.
- [50] Y. Uchino, T. Kobayashi, S. Hasegawa, I. Nagashima, Y. Sunada, A. Manabe, et al., Dependence of the reverse current on the surface of electrode placed on a bipolar plate in an alkaline water electrolyzer, *Electrochemistry* 86 (3) (2018) 138–144.
- [51] R.E. White, C.W. Walton, H.S. Burney, R.N. Beaver, Predicting shunt currents in stacks of bipolar plate cells, *J. Electrochim. Soc.* 133 (1986) 485.
- [52] R.S. Jupudi, G. Zappi, R. Bourgeois, Prediction of shunt currents in a bipolar electrolyzer stack by difference calculus, *J. Appl. Electrochim.* 37 (8) (2007 Aug) 921–931.
- [53] G. Sakas, A. Ibáñez-Rioja, V. Ruuskanen, A. Kosonen, J. Ahola, O. Bergmann, Dynamic energy and mass balance model for an industrial alkaline water electrolyzer plant process, *Int. J. Hydrogen Energy* 47 (7) (2022 Jan 22) 4328–4345.
- [54] S.M. Jung, Y. Kim, B.J. Lee, H. Jung, J. Kwon, J. Lee, et al., Reverse-current tolerance for hydrogen evolution reaction activity of lead-decorated nickel catalysts in zero-gap alkaline water electrolysis systems, *Adv. Funct. Mater.* 2316150 (2024). <https://doi.org/10.1002/adfm.202316150>.
- [55] C. Cremers, T. Jurzinsky, J. Meier, A. Schade, M. Branghofer, K. Pinkwart, et al., DEMS and online mass spectrometry studies of the carbon support corrosion under various polymer electrolyte membrane fuel cell operating conditions, *J. Electrochim. Soc.* 165 (6) (2018) F3307–F3315.
- [56] S.G. Ji, H. Kim, W.H. Lee, H.S. Oh, C.H. Choi, Real-time monitoring of electrochemical carbon corrosion in alkaline media, *J Mater Chem A Mater* 9 (35) (2021 Sep 21) 19834–19839.
- [57] N. Hodnik, P. Jovanović, A. Povlišić, B. Jozinović, M. Zorko, M. Bele, et al., New insights into corrosion of ruthenium and ruthenium oxide nanoparticles in acidic media, *J. Phys. Chem. C* 119 (18) (2015 May 7) 10140–10147.
- [58] S. Cherevko, A.R. Zeradjanin, A.A. Topalov, N. Kulyk, I. Katsounaros, K.J. J. Mayrhofer, Dissolution of noble metals during oxygen evolution in acidic media, *ChemCatChem* 6 (8) (2014) 2219–2223.
- [59] A.R. Zeradjanin, A.A. Topalov, Q. Van Overmeire, S. Cherevko, X. Chen, E. Ventosa, et al., Rational design of the electrode morphology for oxygen evolution-enhancing the performance for catalytic water oxidation, *RSC Adv.* 4 (19) (2014) 9579–9587.
- [60] SB Lyon, 3.21 - Corrosion of Noble Metals, in: Bob Cottis, Michael Graham, Robert Lindsay, Stuart Lyon, Tony Richardson, David Scantlebury, Howard Stott (Eds.), *Shreir's Corrosion*, Elsevier, 2010, pp. 2205–2223.
- [61] S. Cherevko, A.R. Zeradjanin, G.P. Keeley, K.J.J. Mayrhofer, A comparative study on gold and platinum dissolution in acidic and alkaline media, *J. Electrochim. Soc.* 161 (12) (2014) H822–H830.
- [62] M. Schalenbach, O. Kasian, M. Ledendecker, F.D. Speck, A.M. Mingers, K.J. J. Mayrhofer, et al., The electrochemical dissolution of noble metals in alkaline media, *Electrocatalysis* 9 (2) (2018 Mar 1) 153–161.
- [63] A.C. Lazanas, M.I. Prodromidis, *Electrochemical Impedance Spectroscopy—A Tutorial*, vol. 3, ACS Measurement Science Au. American Chemical Society, 2023, pp. 162–193.
- [64] J.O. Majasian, F. Iacoviello, P.R. Shearing, D.J.L. Brett, Effect of microstructure of porous transport layer on performance in polymer electrolyte membrane water electrolyser, in: *Energy Procedia*, Elsevier Ltd, 2018, pp. 111–119.
- [65] G.A. Lindquist, J.C. Gaitor, W.L. Thompson, V. Brodgen, K.J.T. Noonan, S. W. Boettcher, Oxidative instability of ionomers in hydroxide-exchange-membrane water electrolyzers, *Energy Environ. Sci.* 16 (10) (2023 Aug 14) 4373–4387.
- [66] D. Li, A.R. Motz, C. Bae, C. Fujimoto, G. Yang, F.Y. Zhang, et al., Durability of anion exchange membrane water electrolyzers, *Energy Environ. Sci.* 14 (6) (2021) 3393–3419.
- [67] A.Y. Faid, A.O. Barnett, F. Seland, S. Sunde, Highly active nickel-based catalyst for hydrogen evolution in anion exchange membrane electrolysis, *Catalysts* 8 (12) (2018 Dec 1).
- [68] J.A. Bau, S.M. Kozlov, L.M. Azofra, S. Ould-Chikh, A.H. Emwas, H. Idriss, et al., Role of oxidized Mo species on the active surface of Ni-Mo electrocatalysts for hydrogen evolution under alkaline conditions, *ACS Catal.* 10 (21) (2020 Nov 6) 12858–12866.
- [69] M. Dekay Thompson, Albert Kaye, The Electrochemical Oxidation of Molybdenum in Potassium Hydroxide Solutions, *Trans. Electrochim. Soc.* 62 (1932) 255.
- [70] Z. Wang, Y.R. Zheng, J. Montoya, D. Hochfilzer, A. Cao, J. Kibsgaard, et al., Origins of the instability of nonprecious hydrogen evolution reaction catalysts at open-circuit potential, *ACS Energy Lett.* 6 (2021) 2268–2274.
- [71] A.J. Torriero, *Electrochemistry in Ionic Liquids (Fundamentals)*, Springer, Switzerland, 2015.
- [72] P. Trinke, B. Bensmann, R. Hanke-Rauschenbach, Current density effect on hydrogen permeation in PEM water electrolyzers, *Int. J. Hydrogen Energy* 42 (21) (2017 May 25) 14355–14366.
- [73] S.B. Adler, B.T. Henderson, M.A. Wilson, D.M. Taylor, R.E. Richards, Reference electrode placement and seals in electrochemical oxygen generators, *Solid State Ionics* 134 (1–2) (2000 Oct 1) 35–42.
- [74] S.B. Adler, Reference electrode placement in thin solid electrolytes, *J. Electrochim. Soc.* 149 (5) (2002) E166.